Chemical Imaging of Multicomponent Viscous Fingering in Chromatography

Matthew L. Dickson, T. Tucker Norton, and Erik J. Fernandez
Dept. of Chemical Engineering, Thornton Hall, University of Virginia, Charlottesville, VA 22903

Resolution in chromatographic separations can be compromised by nonuniform flow distribution, heterogeneous packing, or flow instabilities such as viscous fingering. In this work, the displacement of solutes within a chromatographic column was monitored with an advanced magnetic-resonance technique, echo-planar spectroscopic imaging (EPSI). Unlike conventional magnetic-resonance imaging, this approach allows multiple solutes to be observed simultaneously, providing separate "chemical images" for each component. Qualitative chemical images were obtained in approximately 1 min with approximately 1 mm^3 spatial resolution. EPSI allowed us to examine the multicomponent viscous fingering problem for the first time. While many features of the instability are preserved, solute retention appears to slow the growth of solvent fingers.

Introduction

The nonuniform flow caused by the viscous fingering flow instability (Homsy, 1987; Yortsos, 1990) has received significant attention primarily because of its importance to enhanced petroleum recovery, but it also impacts groundwater hydrogeology (Held and Illangasekare, 1995), fixed-bed chemical processing, and even medical applications (Bhaskar et al., 1992). In chromatographic and adsorptive separations of viscosity-enhancing solutes, this flow instability can cause serious flow nonuniformities that degrade displacement efficiencies in chromatographic (Flodin, 1961; Moore, 1970; Yamamoto et al., 1986; Plante et al., 1994) and adsorption (Hill, 1952) separations. For example, reduced separation efficiencies due to fingering have been noted with sugars (Hill, 1952; Byers et al., 1990), polymers (Moore, 1970), and proteins (Flodin, 1961; Yamamoto et al., 1986; Plante et al., 1994).

The first experimental demonstration and theoretical analysis of viscous fingering in a miscible displacement is credited to Hill (Hill, 1952). He showed that concentrated sugar solutions could exhibit "channeling" due to viscosity and density differences during sugar purification in fixed beds. Linear stability analysis subsequently revealed that transverse dispersion stabilizes disturbances below a cutoff wavelength and leads to a fastest growing wavelength (Gardner and Ypma, 1984). More recently, the linear stability analyses of miscible fingering have been made more rigorous, incorporating more realistic assumptions including the effects of anisotropic dispersion, velocity-dependent dispersion, and nonmonotonic viscosity profiles (Tan and Homsy, 1986; Yortsos and Zeybek, 1988; Manickam and Homsy, 1993). More complex behavior that cannot be predicted by linear stability analysis, such as fingertip-splitting, finger–finger interactions, permeability heterogeneity, and overall displacement efficiency have been effectively described and studied with numerical simulation (Christie, 1987; Meiburg and Homsy, 1988; Tan and Homsy, 1988; Brock and Orr, 1991; Tchelepi et al., 1993). These numerical models have been compared to experimental results and have been found to represent such data relatively well (Christie et al., 1990). These efforts have produced a rich picture of the complex interplay of microscopic processes and macroscopic forces responsible for viscous fingering dynamics. Recently, numerical simulation has been applied to viscous fingering in packed beds providing insights into the effects of sample properties, operating conditions, and column design on fingering in this context (Norton and Fernandez, 1996). However, the effects of solute adsorption and solute exclusion from pores have not been considered to our knowledge. Such interactions could be significant in many fingering situations, certainly in fixed-bed separations.

Direct experimental visualization of viscous fingering has been hindered by the opaque nature of porous media. Most experimental studies of finger morphology and dynamics in two-dimensional model porous media have involved optical

Correspondence concerning this article should be addressed to E. J. Fernandez.

or X-ray techniques (Hill, 1952; Slobod and Thomas, 1963; Brock and Orr, 1991). Acoustic methods have recently been applied to study fingering in three-dimensional samples, but only with cross-sectional averaging (Bacri et al., 1992). While X-ray-computed tomography has been used to monitor displacements in rock (Vinegar, 1986), no detailed studies concerning fingering have been performed with this method. On the other hand, magnetic resonance imaging (MRI) has been used to visualize viscous fingering in solutions (Pearl et al., 1993), Hele-Shaw cells (Davies et al., 1992), and in conventional packed columns (Athalye et al., 1991; Plante et al., 1994). Recent magnetic-resonance imaging measurements in packed columns have also provided the three-dimensional visualization of viscous fingering in porous media for the first time (Fernandez et al., 1995).

As the name implies, MRI is a derivative of nuclear magnetic resonance (NMR) (Bloch et al., 1946; Purcell et al., 1946). Since the early days of the technique, NMR has been used to measure diffusion (Carr and Purcell, 1954; Stejskal and Tanner, 1965) and other complex displacements such as flow, acceleration, and restricted diffusion (Caprihan and Fukushima, 1990; Callaghan, 1991). These developments have made MRI quite complementary to X-ray-computed tomography methods in studies of flow in porous media (Gummerson et al., 1979; Rothwell and Vinegar, 1985; Vinegar, 1986; Guillot, 1988), particularly in light of advances in quantitative MRI techniques (Caprihan and Fukushima, 1990; Chen et al., 1992; Chen et al., 1994). One disadvantage of conventional MRI visualization of solute transport in porous media, however, is that it is typically based on indirect detection of the solute via the abundant solvent signal. Because only a single signal is collected in this case, similar studies of multicomponent transport are not possible.

In an attempt to overcome this limitation, we have employed a magnetic-resonance approach that combines the spatial and chemical information available from NMR into a single "spectroscopic imaging"experiment (Brown et al., 1982; Maudsley et al., 1983). This strategy has been used to discriminate oil and water in reservoir rock (Horsfield et al., 1990; Majors et al., 1990). While spectroscopic imaging can be extremely time-consuming when using conventional Fourier phase encoding (Kumar et al., 1975) to provide spatial information, echo-planar imaging strategies (Stehling et al., 1991) have been used to accelerate spectroscopic imaging dramatically in a medical context by reducing the number of phase-encoding dimensions required (Posse et al., 1994). In this study, we have tailored this approach to provide the higher spatial resolution required for studies of porous media. This has allowed us to map the spatial distribution of solutes in packed columns during unstable chromatographic displacements of viscous samples containing one and two components. Consequently, we have been able to study the effects of solute retention on the fingering instability. In addition, interactions between fingering patterns for separating bands have been investigated, showing behavior different than for single-component displacements.

Materials and Methods

Size-exclusion chromatography

Glass columns with 3.2 cm ID (Amicon, Beverly, MA) were used for all experiments. The columns were packed with Toyopearl HW-40C size exclusion chromatography media (porous beads of 75-micron (μm) average particle diameter, TosoHaas, Montgomeryville, PA). According to the manufacturer, this material fractionates polyethylene glycol (PEG) with molecular weights in the range of 100 to 3,000 Daltons (Da). 2,3-Butanediol (Sigma) and polyethylene glycol [Fisher (MW 600) and Sigma (MW 1000)] were used as model viscosity-enhancing solutes. The column was slurry packed under flow as recommended by the manufacturer of the chromatography media. The packed-column bed length was 11.5 cm. The packing uniformity was assessed by visualizing the displacement of an MRI contrast agent. The packing uniformity was such that the sample band was never distorted by more than a few mm throughout the length of the column. This distortion was likely due to packing nonuniformities near the inlet, as we have observed previously with this column (Fernandez et al., 1995). The void volume fraction for the column was determined to be approximately 0.4 and the volume including extraparticular and pore volumes was determined to be approximately 0.8, according to solute imaging data. Sample volumes of 4.3 mL were loaded using a six-port injection valve in all experiments. Flow through the column in imaging experiments was carried out at 0.9 mL/min using a peristaltic pump (Gilson model M312, France). A pH 7.0 elution buffer composed of 10 mM sodium phosphate (Fisher), 150 mM sodium chloride (Sigma), and 0.02% w/w sodium azide (Sigma) was used in all column experiments. Chromatographic measurements of butanediol, PEG, and contrast agent retention behavior were performed using a differential refractometer (series R-400, Waters Associates, Milford, MA). Butanediol sample viscosities were measured using a cone-and-plate viscometer (model LVTDCP, Brookfield, Stoughton, MA).

Magnetic-resonance imaging

Magnetic resonance was performed at 74.57 MHz for ^{1}H using a 1.75-T horizontal bore magnet (Nalorac) and console (Tecmag, Houston). MacNMR software (Tecmag, Houston) was used for all NMR experiments. A birdcage resonator (Hayes and Edelstein, 1985), 4 cm in diameter and 10 cm in length, was used for radiofrequency transmission and reception in all of the experiments. Shielded magnetic-field gradients (20 G/cm maximum, Magnex Scientific, Martinez, CA) were used to collect high-quality spin echo (Edelstein et al., 1980) images in short times. Two-dimensional spin echo images (TR = 530 ms; TE = 28 ms; 128 × 128) were collected over a 10.7-cm × 4.3-cm field of view with a total acquisition time of 68 s. Although the sample is being displaced through the column during image acquisition, the resultant blurring of the image is less than might be expected, since most of the large signal intensity data are collected during a short period (perhaps 15 to 30 s) in the middle of the acquisition period. To provide image contrast in MRI experiments with solutes, approximately 10 mM of a gadolinium-based contrast agent (Magnevist, Berlex Laboratories, Wayne, NJ) was included with the injected sample. T_1 values for each sample were obtained by curve-fitting inversion recovery spectra using the MacNMR software. T_2 values were obtained from curve fits of peak intensities of spin echo spectra at 10 to 20 incremented echo times.

Echo-planar spectroscopic imaging

High-speed two-dimensional spectroscopic imaging was performed using the general echo-planar-based procedure of Posse et al. (1994). The pulse sequence used is shown in Figure 1. The experiment is based on a spin echo with an echo time of 10 ms and a repetition time of 0.65 s. Beginning at the top of the echo, a series of 64 readout gradient oscillations applied in the axial direction (G_z) produced 128 gradient echoes whose amplitudes decrease due to the effects of field heterogeneity and T_2 relaxation. Evolution of chemical shift during this time provides the chemical information in the experiment. Thus, in one train of echoes, spatial information in one dimension and chemical information are simultaneously encoded. Because the even and odd echoes traverse k-space in opposite directions, only the odd echoes were acquired and processed. Processing both echoes is complicated by gradient waveform imperfections that can lead to aliasing (Posse et al., 1994). The time between the middle of each odd gradient echo was 2.1 ms, leading to a spectral width of 473 Hz (6.35 ppm) and a spectral resolution of 7.39 Hz (0.099 ppm). Standard slice-selection using a 3-ms three-lobed sinc pulse was performed in one of the transverse directions (G_y), and 64 phase-encoding steps were used in the other transverse direction (G_x). The field of view was 10.7 cm × 4.3 cm. Two signal averages were collected for each phase-encoding step, leading to an acquisition time of 84 s. Magnetic-field homogeneity was optimized using the free-induction decay of the entire object. Field homogeneity was further improved by localized shimming on the y-slice selected for spectroscopic imaging. This localized shimming was performed with a gradient echo excitation using the same slice-selection procedure as carried out for the echo-planar spectroscopic imaging (EPSI) experiment.

EPSI data were processed using IDL (Research Systems, Inc., Boulder, CO). Prior to three-dimensional Fourier transformation, a base-line correction was performed to reduce the effects of DC offset. To reduce truncation artifacts, apodization was performed in both the spatial and spectral dimensions. A weighting function was used equal to unity everywhere except in the final 20% of the data, where a cosine transition was employed. Throughout the spectral dimension, the cosine weight function was also multiplied by a decaying exponential. After Fourier transformation, the data were displayed in the magnitude mode. The effects of magnetic-field variations were corrected partially by frequency shifting the data in the spectral dimension using the water peaks in each spectrum as a chemical shift reference. Images for individual compounds were then produced with IDL using integration between fixed integration limits, as indicated in the text below. The images were bilinearly interpolated from 64×64 resolution to 128×256 resolution using the routine supplied with IDL.

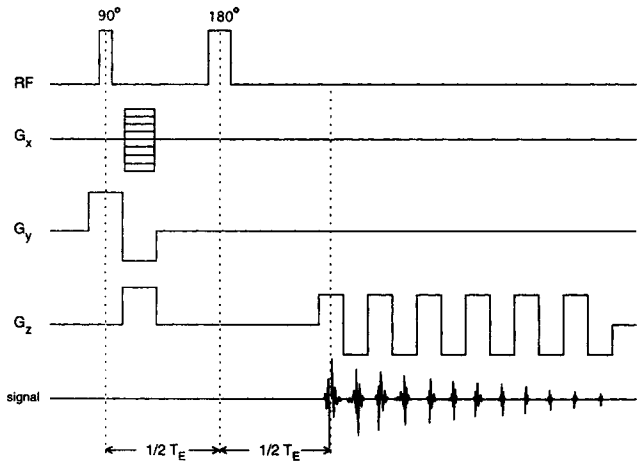

Figure 1. EPSI experiment.

The patterns of gradients applied in the slice selection (G_x), phase encoding (G_y), and readout (G_z) directions are shown. The slice thickness was approximately 2 mm.

Results

Imaging a column using conventional MRI

Figure 2a shows a conventional MR image acquired during elution of a PEG 600 sample through the packed column that was mounted horizontally along the axis of the magnet. The inlet of the column is on the left of the image and the flow is to the right. The MRI signal is derived mainly from water and appears gray everywhere in the column outside the sample band. The signal intensity in the region of the sample band is modified by the enhanced relaxation caused by the gadolinium-containing contrast agent (Magnevist) included in the sample. For the 10-mM concentration of contrast agent used in our samples, the water spin-lattice (T_1) and spin-spin T_2) values for buffer alone and each of the samples with and without contrast agent are shown in Table 1. While the chromatographic particles influence relaxation somewhat, the effect of the contrast agent is the most important contributor to signal reduction in the MR-imaged sample band.

For a 90° excitation pulse, the dependence of the spin echo signal intensity, S, on experimental parameters is given by

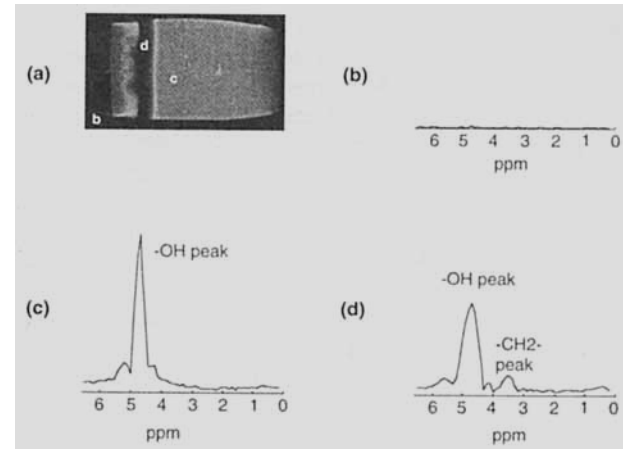

Figure 2. Viscous fingering during the elution of PEG 600.

The 3.2-cm-ID column is positioned horizontally with flow to the right. The sample volume was 4.3 mL and the flow rate was 0.9 mL/min. (a) Conventional magnetic-resonance image of the sample band. ^{1}H magnetic-resonance spectra obtained from a single EPSI data set are shown, at the same scale, for locations (b) outside the column, (c) inside the column out of the sample band, and (d) inside the sample band. Each spectrum is derived from a volume element (voxel) with dimensions (1 mm)^3 at the positions indicated in (a).

Table 1. Relaxation Times of Water for the Solutes Used*

Solute	Conc. (% w/w)	T_1 (ms)		T_2 (ms)	
		Gd	No Gd	Gd	No Gd
Elution buffer		26.67±0.57	475.80±15.74	6.88±0.37	49.79±0.96
2,3-Butanediol	30	12.70±0.25	347.62±1.06	4.37±0.07	31.92±0.80
PEG 600	20	15.85±0.50	—	5.69±0.10	—
2,3-Butanediol +PEG 600	30+20	6.12±0.16	—	2.04±0.01	—

*All measurements were made in HW40C medium. When added, contrast agent concentrations were 10 mM.

$$S(x,y,z) \propto \rho(x,y,z)e^{-TE/T_2}\{1-e^{-TR/T_1}\}, \qquad (1)$$

where ρ is the concentration of ^{1}H nuclei (Waugh, 1970; Haase, 1990). Equation 1 describes how the reduction of the water T_1 increases signal recovery during the repetition time (TR) and reduction of water T_2 reduces the signal during the spin echo time (TE). Indeed, the very short T_2 of the samples used here (2 to 7 ms, see Table 1) caused the signal to be completely lost during the spin echo time of the MRI experiment (28 ms). Thus, the region of high gadolinium concentration at the center of the sample band appears black in Figure 2a. At the edges of the sample band where the contrast-agent concentration is reduced, T_1 enhancement dominates and the MRI signal was enhanced considerably. Equation 1 could be used to quantitate the sample concentration at a particular point if the relaxation times can be determined for each time point. However, this process is time-consuming given the speed of the moving sample bands. Alternatively, a calibration curve can be obtained (Fernandez et al., 1995). In any case, these approaches can only easily identify a single solute based on the single water signal.

Although the image from Figure 2a does not directly provide the concentration distribution of solute, the edges of the sample band clearly indicate penetration of solvent into the rear of the sample band as expected for this viscous sample. The leading edge of the sample band is stable to any flow disturbances. As we have observed previously, the stability of this leading edge actually "irons out" flow nonuniformities due to heterogeneous column packing or poor flow distribution (Fernandez et al., 1995).

This MRI approach for visualizing the distribution of molecules can be effective when the molecules are of similar size and retention properties. This technique might not be expected to work with large molecular-weight polymers, since they may have a measurably larger molecular size than the contrast agent, which is presumably compactly arranged around its gadolinium ion. Examination of the PEG 600 elution curve indicates that gadolinium and PEG very nearly coelute from the column (data not shown).

Imaging a column using EPSI

In a separate experiment using the same column, the displacement of a PEG 600 sample without contrast agent was monitored using the EPSI technique. Because magnetic-resonance spectroscopic imaging techniques incorporate the chemical information available from NMR, EPSI provides a chemical analysis at multiple points throughout the sample, in this case our column. For example, Figures 2b–2d show spectra obtained from one EPSI experiment performed at the same elution volume as the conventional MRI in Figure 2a. The spectra in Figure 2 reveal the chemical composition of volume elements (voxels) approximately (1 mm)^3 in size. Figure 2b is a spectrum obtained at a position outside the object, showing no signals present. The spectrum of Figure 2c represents the composition at a point inside the column but outside the sample band. In this spectrum a single strong signal due to the solvent water is evident. Inside the sample band, Figure 2d shows a large signal due to ^{1}H nuclei in water with a small contribution from the hydroxyl ^{1}H nuclei at the ends of the PEG molecule. In addition, a smaller signal at 3.5 ppm is due to the four aliphatic ^{1}H nuclei composing the $-CH_2CH_2O-$ monomeric unit of PEG. The spectra in Figures 2b–2d have a spectral resolution of approximately 7.5 Hz (0.1 ppm) per point. This value is limited by the number of echoes acquired here and the magnetic-field homogeneity in some regions of the sample, particularly near the ends of the column. Although the spectral resolution is relatively low compared with typical analytical NMR, the spectral resolution is sufficient to resolve the hydroxyl resonance and the aliphatic resonance of PEG. PEG and butanediol were chosen in part because their NMR spectra were simple and included resonances well resolved from water and from each other.

The spectra obtained via EPSI could be used to quantify the amount of water and solutes present in each voxel because the NMR peak areas are linearly proportional to the amount of each nucleus present. However, there are significant challenges to doing this. First, the proportionality between peak area and concentration can be different for each nucleus, because of the effects of relaxation. Porous media can have a significant effect on relaxation, particularly where strong adsorption is involved. Fortunately, in our EPSI experiments there is little adsorption of the solutes to the size exclusion chromatography media, and relaxation times are likely to be more spatially uniform since contrast agents are not involved. A second obstacle to quantitation is magnetic-field inhomogeneities on macroscopic and pore-length scales, which can shift and distort peak shapes considerably. For example, this is the main reason for the differences in $-OH$ peak shapes between the spectra shown in Figures 2c and 2d. While field inhomogeneities may not alter the peak area, they can confound attempts to measure peak areas. Field inhomogeneities and efficient T_2 relaxation will also cause a rapid decrease in the signal during the EPSI echo train, which will lead to some additional spatial apodization and smoothing of the image in the readout direction (z-direction in our case).

We have not attempted to take all these effects into account, but we have constructed qualitative images of solute distributions in the column by integrating the peak areas af-

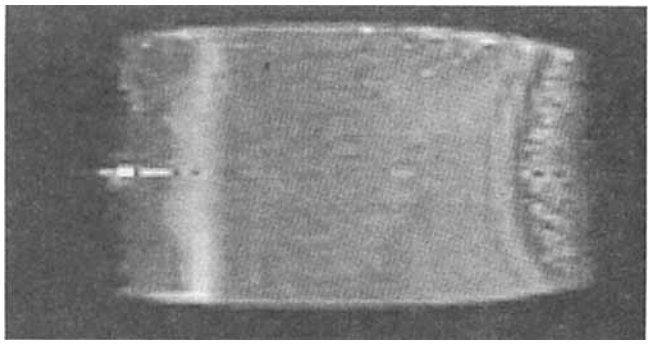

Figure 3. Spectroscopic image of the PEG 600 distribution obtained with EPSI.

The inlet appears on the left side of the image and flow is to the right.

ter partial correction of field homogeneity effects (see the Materials and Methods section). Figure 3 shows such an image constructed for PEG 600 obtained from the EPSI experimental data highlighted in Figures 2b–2d. In this image, the intensity is proportional to the integral of the magnetic-resonance spectrum between 3.2 and 3.8 ppm. The intrinsic spatial resolution in the EPSI image is approximately half that of the conventional MR image, although the data have been bilinearly interpolated for display in Figure 3. Consistent with the location of the sample band indicated by the MRI in Figure 2a, the EPSI image intensity is low throughout the body of the column and is high in the sample band region. Outside of the sample band region, image intensity is also present that we attribute to the strong water peak. Although spectra obtained in these regions of the column reveal only the single water peak (as in Figure 2c), the tails of the water peak extend slightly into the integration region of the aliphatic proton peak and contribute a significant area due to the large amplitude of the water signal (e.g., compare signal present in the $-CH_2-$ peak region in Figure 2c to Figure 2b). This tailing was exacerbated by the magnitude calculation used to process the data. Near the ends of the column the individual spectra reveal that the water and aliphatic proton peak widths are substantially broadened due to substantial magnetic-field heterogeneity. This broadening is likely due to magnetic-field susceptibility differences between the column packing (water and polymeric beads) and the air and plastic column components beyond the ends of the bed. Peak broadening is also responsible for the apparent "ringing" observed in the EPSI images at the right side of the column.

Imaging the displacement of a small molecule

To compare the information available from MRI and EPSI about viscous fingering during an entire chromatographic displacement, the elution of a small molecule was monitored by both methods. In one experiment the displacement of a 30% v/v butanediol sample in elution buffer was visualized using conventional MRI by including a contrast agent in the sample. In a subsequent experiment, EPSI was used to follow the displacement of a butanediol sample that did not contain a contrast agent. The viscosity of these and the other samples used in this study are shown in Table 2. Conventional magnetic resonance images and images obtained with EPSI for

Table 2. Viscosities of Samples Used*

Solute	Concentration (% w/w)	Viscosity (cp) Gd	Viscosity (cp) No Gd
2,3-Butanediol	30	3.99±0.05	3.87±0.05
PEG 600	20	2.94±0.03	2.82±0.04
PEG 1000	20	3.54±0.08	3.56±0.04
2,3-Butanediol + PEG 600	30+20	13.3±0.3	12.6±0.3
2,3-Butanediol + PEG 1000	30+20	15.5±0.2	15.2±0.5

*Readings are shown in cp with standard deviations for six readings at different shear rates. None of the solutions showed shear-rate dependence.

2,3-butanediol are shown in Figures 4a and 4b, respectively. Each of the images is taken from a horizontal slice along the axis of the column. The EPSI images were obtained by integrating the spectra in each data set between 0.7 and 1.5 ppm. In each set of images, two dominant fingers are formed near the walls of the column and weaker fingering is observed in the center. This pattern is initiated by the nonuniform flow pattern at the column inlet caused by the flow distributor and a region of nonuniform packing. This pattern of flow nonuniformity and fingering is consistent with our previous experience with this column design (Fernandez et al., 1995).

Unfortunately, conventional MRI may not be used to conclusively study the fingering behavior of butanediol at later elution times. A comparison of the MRI and EPSI results in Figure 4 indicates that the sample band does not migrate at

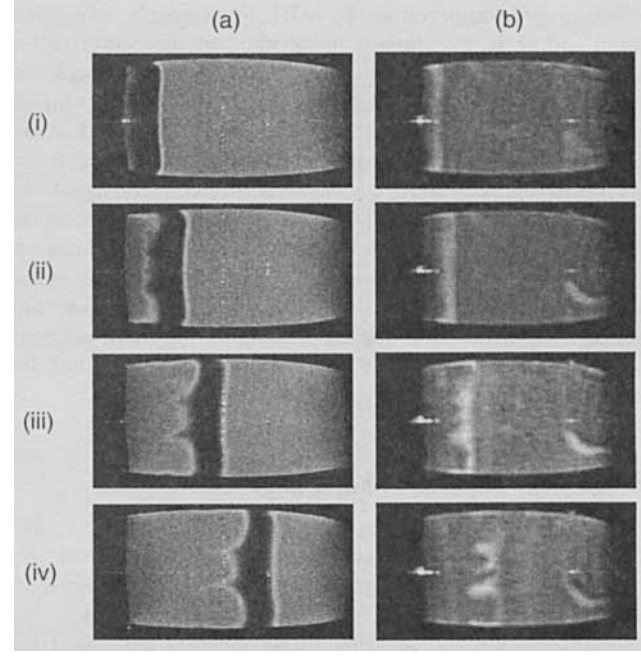

Figure 4. Time course of 2,3-Butanediol elution visualized with (a) MRI and (b) EPSI.

The two series were collected on subsequent displacements without repacking the column. The conditions for the displacements were identical except that the sample did not contain contrast agent in the EPSI experiment. A new image was acquired every two minutes. The field of view is 10.7 cm × 4.3 cm and 11.6 cm × 3.9 cm for the MRI and EPSI images, respectively. Flow is to the right. Images i, ii, iii, and iv, respectively, correspond to elution times of 6, 10, 16, and 24 minutes after sample injection.

the same rate in each set of images. Chromatographic data show that the butanediol is retained more strongly on the column than the contrast agent (data not shown), despite the fact that both of these molecules are relatively small compared to the pore size of the material. Butanediol has a greater retention time than an injected sample of salt, indicating that butanediol adsorbs onto the SEC material. Thus, unlike the MR image, the EPSI images are more valuable in this case because they *directly* monitor the butanediol as it is displaced through the column. This explains why small-amplitude fingers with wavelengths of a few millimeters are present in both types of images (Figure 4a-ii and Figure 4b-ii) early in the time course when the butanediol and contrast-agent bands still overlap, and why the finger patterns are different for the two sets of images at later times.

Thus, the more reliable EPSI images in Figure 4b may be used to analyze the fingering behavior of butanediol, albeit at lower spatial resolution than the MR images. The EPSI spatial resolution is lower because only the ^{1}H nuclei from one of the solutes (e.g., ca. 20 M ^{1}H nuclei for 30% v/v butanediol) are used to construct individual chemical images rather than abundant nuclei from water (ca. 100 M ^{1}H nuclei). In addition, the solute signal intensity can also be reduced somewhat by J-coupling, although the echo time has been limited to 10 ms to minimize this effect. In any case, the lower signal available for the solutes requires that the spatial resolution be sacrificed to provide adequate signal-to-noise ratio in the images.

Despite the lower resolution of the EPSI images, there appears to be some finer structure in the solvent fingers in the EPSI images compared to the MRI. For example, in Figures 4b-iii and 4b-iv, two fingers are evident in the center of the sample-band trailing edge. The finer structure is consistent from image to image and is not simply due to the random noise. Also, the wavelengths of the fingers observed in the later EPSI images are similar to the finger wavelengths observed in the early MR images, when the contrast agent and butanediol bands are similar in location. Another difference between the EPSI and conventional MRI is the thinner appearance of the sample band in the EPSI images. This is due to the nonlinear relationship between signal intensity and solute concentration in the MRI images. The dark edges of the sample band in the MRI correspond to less than half the maximum solute concentration.

Imaging the displacement of a large molecule

To determine the effects of solute retention on the viscous fingering instability, displacements of polyethylene glycol were performed. Based on its larger size, PEG should elute more quickly than butanediol. Figure 5 displays the results of two experiments conducted using MRI (Figure 5a) and EPSI (Figure 5b) to visualize the displacement of a 20% (w/w) PEG sample with an average molecular weight of 600. A comparison of the positions of the PEG sample band in the MRI and EPSI images in Figure 5 demonstrates that the two solutes migrate at similar velocities and have similar fingering-induced signal profiles. In the spectroscopic images of Figure 5b, the image intensity is proportional to the integral of magnitude signal intensity in the region between 2.5 and 3.5 ppm of the ^{1}H NMR spectrum. The PEG 600 band is clearly visible as it loads onto the column, and solvent penetration into the rear of the sample band is also readily apparent. A similar pattern of fingers invading the PEG band is observed using EPSI compared to MRI, although the pattern is less distinct with EPSI because of its lower spatial resolution. In the spectral dimension of the data, the tails of the large water peak contribute to the integrated PEG 600 signal, leading to image intensity in regions of the column outside the PEG sample band. In this run, magnetic-field distortions also produced stationary dark rings observed near the outlet of the column. These artifacts are more pronounced in the PEG images than in the previous butanediol images because the PEG methylene resonance is much closer to the water resonance in the spectral dimension than is the methyl resonance of 2,3-butanediol.

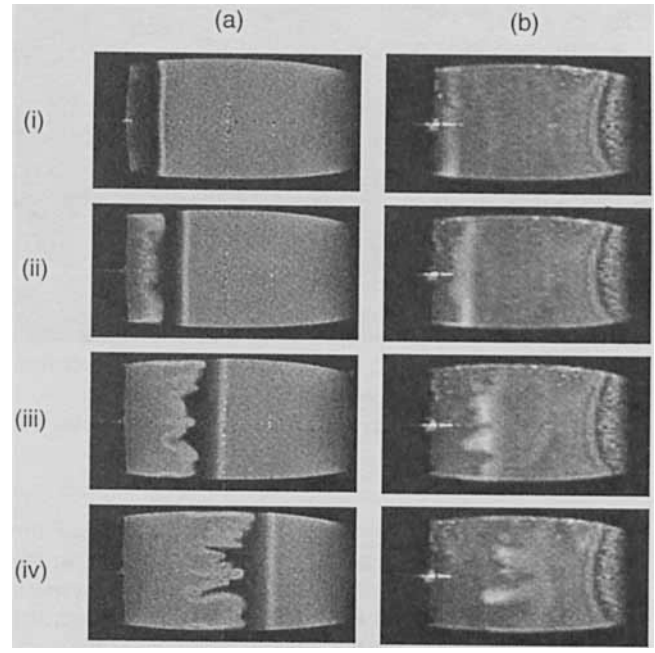

Figure 5. Time course of PEG 600 elution monitored with (a) MRI and (b) EPSI.

Imaging parameters and times are the same as Figure 4. Sample volume, 4.3 mL; solute concentration, 20% w/w; flow is to the right.

While the general three-lobed pattern of fingering in the PEG 600 sample in Figure 5 is similar to that of butanediol (Figure 4b), there are dramatic differences in the finger morphology and dynamics. The finger wavelengths evident in the later images are smaller for PEG 600 compared to butanediol (e.g., compare Figure 5b-iii with 4b-iv). Also, the finger growth rates are higher for PEG 600 (e.g., compare Figure 4b-iv and Figure 3b-iv). These differences in fingering patterns are presumably due to a combination of differences in the viscosity, solute retention, and molecular diffusivity of the two samples.

To determine the effect that a sample of even higher molecular size would have on the development of viscous fingers, the displacement of PEG 1000 was investigated. MRI of a 20% w/w PEG 1000 sample are shown in Figure 6a. The fingering pattern again shows three clusters of fingers at the top, middle, and the bottom of the sample's trailing edge, but

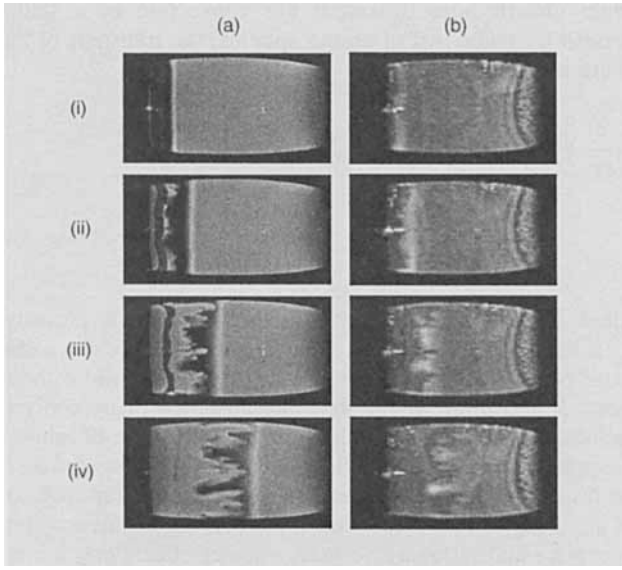

Figure 6. Time course of PEG 1000 elution monitored with (a) MRI and (b) EPSI.

Imaging parameters and times are the same as Figure 4. Sample volume, 4.3 mL; solute concentration, 20% w/w; flow is to the right.

the finger growth rates are somewhat higher for PEG 1000 than for PEG 600 or butanediol. One unusual feature of the MR images in Figures 6a-ii and 6a-iii is a second band of lower (darker) image intensity, indicating the presence of an additional component that is displaced at a slower rate. Because this band was not observed in the PEG 600 case, it is possible it may be related to a contaminant in the PEG 1000 or contrast agent. However, this contaminant must be present in low concentrations, as it does not appear in high-resolution NMR spectra (data not shown) or the PEG 1000 EPSI images (see Figure 5b). A comparison of the PEG bands displayed in the EPSI and conventional MR images demonstrates that PEG 1000 and contrast agent appear to coelute in the column. The elution curves of a mixture of PEG 1000 and contrast agent also confirm that the two solutes approximately coelute (data not shown). However, small differences in elution times between the contrast agent, PEG 600, and PEG 1000 make interpretation of the MRI difficult.

The EPSI images show general fingering patterns for PEG 1000 that do match well with the PEG 600, although the growth rates are higher. Compared to the butanediol EPSI images (Figure 4b), the PEG 1000 definitely shows stronger finger growth and narrower finger wavelengths even though the viscosities are nearly identical (see Table 2). However, butanediol displays wider fingers than PEG 1000 despite the fact that PEG 1000 is less viscous. Presumably, this disparity must be a result of the differences in molecular diffusivity and solute retention between butanediol and PEG.

Viscous fingering during two component separations

The effect of two interacting viscous bands was investigated in two elutions of butanediol/PEG sample mixtures

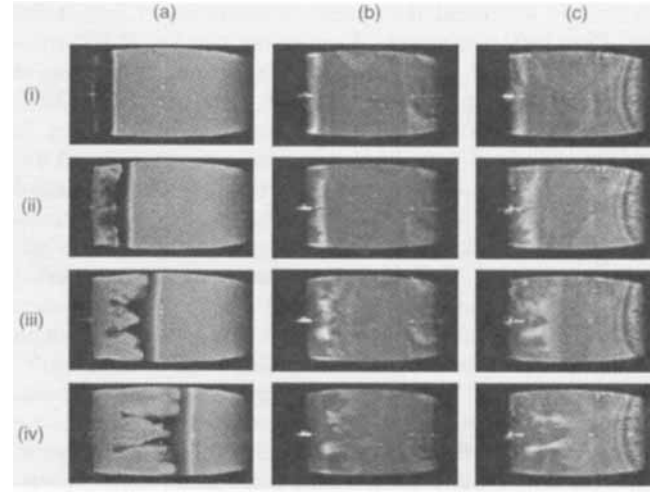

Figure 7. Time course of 2,3-Butanediol (30% w/w) and PEG 600 (20% w/w) elution monitored with MRI and EPSI.

(a) Conventional MR images, (b) EPSI butanediol images, (c) EPSI PEG 600 images. Imaging parameters and times are the same as Figure 4. Sample volume, 4.3 mL; flow is to the right.

monitored by conventional MRI and EPSI. In each case, the 4.3-mL sample contained 30% w/w butanediol and either 20% w/w PEG 600 or 20% w/w PEG 1000. Because these samples contained each of the components at concentrations identical to the single component experiments cited earlier, the mixed samples had substantially higher viscosities (as seen in Table 2). As expected, MR images show that finger growth for the mixed samples containing PEG 600 (Figure 7a) and PEG 1000 (Figure 8a) outpace that of either single-component displacement (Figures 4b and 5b).

Whereas two solutes of interest cannot be distinguished in conventional MR images, the spectroscopic images of Figures

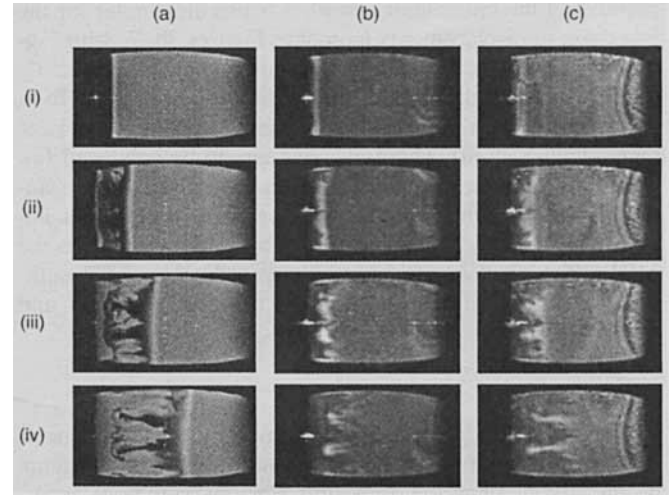

Figure 8. Time course of 2,3-Butanediol (30% w/w) and PEG 1000 (20% w/w) elution monitored with MRI and EPSI.

(a) Conventional MR images, (b) EPSI butanediol images, (c) EPSI PEG 1000 images. Imaging parameters and times are the same as Figure 4. Sample volume, 4.3 mL; flow is to the right.

7b and 7c do reveal the spatial distributions of butanediol and PEG 600, respectively. Even in the first set of EPSI images (Figures 7b-i and 7b-ii), the different migration rates of the two components can be detected. As expected, the PEG 600 migrates more quickly than the butanediol. Figures 7b and 7c also show that the distortions in the PEG band are larger in amplitude than the distortions in the butanediol band throughout the displacement of the two components. Although the spectroscopic images are not as clear as the MR images, the EPSI images suggest that the butanediol leading edge is initially relatively flat (Figure 7b-i), but soon begins to show substantial distortion (Figures 7b-ii through 7b-iv). This unstable flow at the leading edge of the butanediol band contrasts with the single-component behavior and is caused by the passage of the butanediol band through the fingering zone at the rear of the PEG 600 band as the separation occurs. Clearly there will be a complex viscosity distribution throughout the bed, and when the components begin to resolve from one another, there will be a minimum in viscosity between the separating bands. This could potentially provide a stabilizing influence for the leading edge of the butanediol band, which could dampen the growth of the instability.

A separation of butanediol from a larger molecular-weight polymer, PEG 1000, is shown in Figure 8. Conventional MR images (Figure 8a) show that this mixed sample exhibits faster finger growth than any of the previous samples, consistent with the 20% higher viscosity of this mixed sample compared to the PEG 600 + butanediol sample (see Table 2). The MR images also show a second contaminating band as was observed in the single-component PEG 1000 displacement (Figure 6a).

The pattern of fingering into the contrast agent band is somewhat different from the pattern seen in the separation involving PEG 600 (Figure 7a). This could be due to differences in sample viscosity, but the different retention of the PEG 600 and PEG 1000 could also be responsible. The EPSI images of Figure 8b show that the wavelengths and fingering patterns of the butanediol and PEG bands are similar for the two types of displacements (compare Figures 7b, 7c with Figures 8b, 8c). However, the mixed samples exhibit significantly smaller wavelengths for the butanediol band (Figures 7b-iii and 8b-iii) than in the single-component butanediol displacement (Figure 4b-iii). There also appears to be enhanced finger coalescence in the PEG EPSI images of the mixed sample compared with the corresponding single-component images. This "enhanced coalescence" is also quite evident in the MRI, although it is difficult to interpret because of the differences in migration rate between the contrast agent and the solutes.

Discussion

To our knowledge, this is the first study that has considered the effects of solute retention and multiple components on the viscous fingering instability. For the conditions examined here, the more retained butanediol exhibited slower solvent finger growth compared to the PEG samples. The addition of a second, separating solute also modified the behavior of the instability compared with single-component displacements. In this study, the EPSI technique has provided useful complementary information to MRI.

While the decrease in finger growth rate for butanediol could be related to a slightly lower molecular diffusivity than PEG 600 or 1000, its greater retention can explain the lower finger growth rates observed. For convection of a solute through a packed bed of porous spheres, the transport of the solute is given by

$$\alpha\frac{\partial c_i}{\partial t} + K_{d_i}(1-\alpha)\epsilon\frac{\partial c_i^*}{\partial t} + \rho_s(1-\alpha)(1-\epsilon)\frac{\partial q_i}{\partial t} + \alpha\frac{\partial(vc_i)}{\partial z} - \alpha D\frac{\partial^2 c_i}{\partial z^2} = 0, \quad (2)$$

where α is the bed porosity; ϵ is the intraparticle porosity; K_d is the accessible pore fraction for solute i; ρ_s is the solid-phase particle density, that is, the density of the solid without pores; c_i and q_i are the mobile and adsorbed phase concentrations, respectively; c_i^* is the pore concentration of solute i in equilibrium with the mobile-phase concentration; and D is the dispersion coefficient, defined as the sum of the molecular and eddy diffusivities (Wankat, 1986). For the case where adsorptive and intraparticle mass-transfer effects may be neglected, the two-porosity model may be recast in the form

$$\left[1 + K_{d_i}\frac{(1-\alpha)}{\alpha}\epsilon\right]\frac{\partial c_i}{\partial t} + v\frac{\partial c_i}{\partial z} - D\frac{\partial^2 c_i}{\partial z^2} = 0, \quad (3)$$

where the coefficient of the time derivative now includes the contributions due to pore holdup mechanisms. The coefficient in parentheses in Eq. 4 is a constant factor by which the solute and interstitial velocities differ and can be used to rescale the time variable. If we rescale the time variable in this way, we regain the convection dispersion equation used by Chouke in his linear stability analysis (Gardner and Ympa, 1984). Thus, the wavelengths of fingers would be unchanged and the growth rates would be altered by the time-stretching factor. However, because the fingering time scale for a retained solute is stretched by the same factor as the chromatographic retention, the fingering amplitudes *at the same point on the column* should be the same for two solutes with different retention properties. This is borne out by the experiments here for single solutes (for an approximate comparison, see Figures 4b-iii, 5b-iii, and 6b-iii). This trend should also be true for an adsorbing solute with a linear isotherm.

This argument, however, does not explain the differences in wavelengths observed for PEG compared with butanediol. A linear stability analysis of miscible displacement provided by Chouke gives a fastest growing wavelength of

$$\lambda_{\max} = \frac{2\pi}{\sqrt{5}-2}\left(\frac{\mu_{\text{sample}} + \mu_{\text{solvent}}}{\mu_{\text{sample}} - \mu_{\text{solvent}}}\right)\frac{D_T}{V}, \quad (4)$$

where μ is viscosity, D_T is the transverse dispersion coefficient, and V is the superficial velocity (Gardner and Ypma, 1984). Thus, the larger viscosity of the butanediol samples compared to PEG 600 would be expected to result in smaller wavelengths for butanediol, in contrast to what is observed. Growth rates estimated by linear stability analysis are also predicted to be higher for samples with greater viscosities

(Tan and Homsy, 1986), contrary to the experimental observations of Figures 4 and 5. In addition to having different solute retention, PEG 600 could have a measurably lower diffusivity than butanediol given its larger molecular size. Under these low *Pe* conditions ($Vd_p/D_0 \sim 10$, where d_p is particle diameter and D_0 is the molecular diffusivity), the contribution of molecular diffusivity to transverse dispersion could be measurable (Perkins and Johnston, 1963) and could contribute to the differences in observed wavelengths (Norton and Fernandez, 1996).

Solute retention also has interesting consequences for multicomponent separations where more than one viscous sample band is present. The results here show that the separation of two viscosity-enhancing solutes results in modified fingering behavior compared with single-component displacements. Modifications include deformation of the leading edge of the trailing band, enhanced overall fingering, and possibly enhanced finger coalescence. The effects of complex and nonmonotonic viscosity profiles have been recently examined and found to have a significant impact on the instability (Manickam and Homsy, 1993); however, further investigation is necessary to assess the relative importance of retention, sample volume, dispersion, and intraparticle mass-transfer effects on fingering during separation.

This study also highlights the advantages and limitations of using conventional MRI and EPSI to visualize transport in porous media. Both MRI and EPSI can be used to visualize elution of single components within a column and nonuniform flow that occurs during viscous fingering. Because MRI is based on the entire ^{1}H signal including the abundant solvent, high spatial-resolution and/or high signal-to-noise images can be obtained. Hence, for single-component displacements in which appropriate contrast agents can be incorporated, MRI is an effective way to study the details of fingering in three-dimensional porous media. In contrast, at the expense of reduced signal-to-noise and/or spatial resolution, EPSI can directly detect solutes of interest and provides the new ability to detect the spatial distribution of multiple solutes simultaneously, in acquisition times of approximately one minute when the concentrations of the solutes are high enough. Moreover, this information is available without the need for paramagnetic labels that may alter the solute physicochemical properties.

While EPSI spectra in which peak areas are directly proportional to the concentration of the solute present in any voxel, the measurement and conversion of these peak areas into absolute concentrations is a significant challenge. Complex relaxation behavior in ideal and realistic porous media can alter the proportionality constants relating peak area and concentration. Magnetic-field inhomogeneities can broaden and distort peak shapes, requiring careful integration or peak fitting procedures for accurate measurement. Fortunately, improved quantitation strategies developed for medical applications of conventional spectroscopic imaging are available that often incorporate field and lineshape correction strategies (de Graaf et al., 1990; Horsfield et al., 1990; Kreis et al., 1993; Maudsley et al., 1994). It should be noted that peak broadening due to relaxation or field inhomogeneity will reduce spectral resolution and limit the number and complexity of compounds that can be examined by ^{1}H EPSI.

Careful choice of porous media materials and geometries can minimize the effects of susceptibility differences. Automatic field optimization methods would also improve the overall field homogeneity. Under these conditions, careful measurements of peak area would likely provide accurate relative solute concentrations. Other nuclei that have a larger chemical shift range such as ^{13}C, ^{15}N, or ^{19}F could also be considered to improve spectral resolution and eliminate solvent signals if they are undesired. The Dixon method for spectroscopic imaging might be considered for simple cases with two components (Dixon, 1984); however, the rapid decay of transverse magnetization during the chemical shift evolution period as well as phase errors induced by field inhomogeneity would need to be corrected through improved experimental design and/or postprocessing of the data.

Conclusions

We have shown that high-speed magnetic-resonance spectroscopic imaging can be successfully used to monitor multicomponent transport in porous media *in situ*. Although the chemical images obtained by the EPSI technique are only qualitative at this point, EPSI has permitted visualization of multiple components simultaneously during viscous fingering for the first time. Single-component experiments indicate that increased solute retention acts to decrease finger growth rate. The presence of multiple viscosity-enhancing solutes appears to alter the general trends in finger dynamics. In binary separations of viscosity-enhanced solutes, fingering is observed in the leading edge of the slower migrating component and the finger wavelengths of both components are notably different in the presence of the second component, possibly due to enhanced finger coalescence. However, further study is required to evaluate the effects of retention and multiple components on the multicomponent viscous fingering instability. While spectroscopic imaging has limitations, it provides a new way to study complex transport multicomponent problems, particularly involving solutes at high concentrations in opaque media, allowing us to more thoroughly address the effect that these chromatography properties have on viscous fingering dynamics.

Acknowledgments

This work was supported by the Donors of the American Chemical Society/Petroleum Research Fund, the National Science Foundation (BCS-9210199), and DuPont. The authors thank M. Douglas LeVan and Donald Kirwan for helpful discussions.

Literature Cited

Athalye, A. M., S. J. Gibbs, and E. N. Lightfoot, "Predictability of Size-Exclusion Chromatography for Protein Separation," AIChE Meeting, Los Angeles (1991).

Bacri, J. C., N. Rakotomalala, D. Salin, and R. Woumeni, "Miscible Viscous Fingering—Experiments Versus Continuum Approach," *Phys. Fluids A*, **4**, 1611 (1992).

Bhaskar, K. R., P. Garik, B. S. Turner, J. D. Bradley, R. Bansil, H. E. Stanley, and J. T. LaMont, "Viscous Fingering of HCl Through Gastric Mucin," *Nature*, **360**, 458 (1992).

Bloch, F., W. W. Hansen, and M. Packard, "Nuclear Induction," *Phys. Rev.*, **69**, 127 (1946).

Brock, D. C., and F. M. Orr, Jr., "Flow Visualization of Viscous Fingering in Heterogeneous Porous Media," SPE Tech. Meeting, Dallas (1991).

Brown, T. R., B. M. Kincaid, and K. Ugurbil, "NMR Chemical Shift Imaging in Three Dimensions," *Proc. Nat. Acad. Sci. USA*, **79**, 3523 (1982).

Byers, C. H., W. G. Sisson, J. P. I. DeCarli, and G. Carta, "Sugar Separations on a Pilot Scale by Continuous Annular Chromatography," *Biotechnol. Prog.*, **6**, 13 (1990).

Callaghan, P. T., *Principles of Nuclear Magnetic Resonance Microscopy*, Oxford University Press, New York (1991).

Caprihan, A., and E. Fukushima, "Flow Measurements by NMR," *Phys. Rep.*, **198**, 195 (1990).

Carr, H. Y., and E. M. Purcell, "Effects of Diffusion on Free Precession in Nuclear Magnetic Resonance Experiments," *Phys. Rev.*, **94**, 630 (1954).

Chen, S., K.-H. Kim, F. Qin, and A. T. Watson, "Quantitative NMR Imaging of Multiphase Flow in Porous Media," *Magn. Reson. Imaging*, **10**, 815 (1992).

Chen, S., F. Qin, and A. T. Watson, "Determining Fluid Saturations during Multiphase Flow Experiments by NMR Imaging Techniques," *AIChE J.*, **40**, 1238 (1994).

Christie, M. A., "Numerical Techniques for High-Resolution Simulation of Instabilities," *Soc. Petrol. Engrs. Reservoir Eng.*, **4**, 297 (1989).

Christie, M. A., A. D. W. Jones, and A. H. Muggeridge, "Comparison between Laboratory Experiments and Detailed Simulations of Unstable Miscible Displacement Influenced by Gravity," *North Sea Oil & Gas Reservoirs II (Proc. of North Sea Oil and Gas Reservoirs Conf., Trondheim, Norway, 1989)*, E. B. Antony, T. Buller, O. Hjelmeland, J. Kleppe, O. Torsaeter, and J. O. Aasen, eds., Graham and Trotman, London (1990).

Davies, E. S., T. P. L. Roberts, T. A. Carpenter, L. D. Hall and C. Hall "Visualization of Viscous Fingering by Nuclear Magnetic Resonance Imaging," *J. Magn. Reson.*, **96**, 210 (1992).

de Graaf, A. A., J. E. van Dijk, and W. M. M. J. Bovée, "QUALITY: Quantification Improvement by Converting Lineshapes to the Lorentzian Type," *Magn. Reson. Med.*, **13**, 343 (1990).

Dixon, W. T., "Simple Proton Spectroscopic Imaging," *Radiology*, **153**, 189 (1984).

Edelstein, W. A., J. M. S. Hutchison, G. Johnson, and T. Redpath, "Spin Warp NMR Imaging and Applications to Human Whole-Body Imaging," *Phys. Med. Biol.*, **25**, 751 (1980).

Fernandez, E. J., C. A. Grotegut, G. W. Braun, K. J. Kirschner, J. R. Staudaher, M. L. Dickson, and V. L. Fernandez, "The Effects of Permeability Heterogeneity on Miscible Viscous Fingering: A Three-Dimensional Magnetic Resonance Imaging Analysis," *Phys. Fluids A*, **7**, 468 (1995).

Flodin, P., "Methodological Aspects of Gel Filtration with Special Reference to Desalting Operations," *J. Chromatogr.*, **5**, 103 (1961).

Gardner, J. W. and J. G. J. Ympa, "An Investigation of Phase-Behavior/Macroscopic-Bypassing Interaction in CO_2 Flooding," *Soc. Pet. Eng. J.*, **24**, 508 (1984).

Guillot, G., "Magnetic Resonance Imaging of Liquids in Porous Media: A Comparison to Other Visualization Techniques," *Disorder and Mixing*, Vol. 152, E. Guyon, J.-P. Nadal, and Y. Pomeau, eds., Kluwer, London (1988).

Gummerson, R. J., C. Hall, W. D. Hoff, R. Hawkes, G. N. Holland, and W. S. Moore, "Unsaturated Water Flow Within Porous Materials Observed by NMR Imaging," *Nature*, **281**, 56 (1979).

Haase, A., "Snapshot FLASH MRI. Applications to T1, T2, and Chemical-Shift-Imaging," *Magn. Reson. Med.*, **13**, 77 (1990).

Hayes, C. E., and W. A. Edelstein, "An Efficient, Highly Homogeneous Radiofrequency Coil for Whole-Body NMR Imaging at 1.5 T," *J. Magn. Reson.*, **63**, 622 (1985).

Held, R. J., and T. H. Illangasekare, "Fingering of Dense Nonaqueous Phase Liquids in Porous-Media: 1. Experimental Investigation," *Water Resour. Res.*, **31**, 1213 (1995).

Hill, S., "Channelling in Packed Columns," *Chem. Eng. Sci.*, **1**, 247 (1952).

Homsy, G. M., "Viscous Fingering in Porous Media," *Annu. Rev. Fluid Mech.*, **19**, 271 (1987).

Horsfield, M. A., C. Hall, and L. D. Hall, "Two-Species Chemical-Shift Imaging Using Prior Knowledge and Estimation Theory. Application to Rock Cores," *J. Magn. Reson.*, **87**, 319 (1990).

Kreis, R., T. Ernst, and B. D. Ross, "Absolute Quantitation of Water and Metabolites in the Human Brain. II. Metabolite Concentrations," *J. Magn. Reson. B*, **102**, 9 (1993).

Kumar, A., D. Welti, and R. R. Ernst, "NMR Fourier Zeugmatography," *J. Magn. Reson.*, **18**, 69 (1975).

Majors, P. D., J. L. Smith, F. S. Kovarik, and E. Fukushima, "NMR Spectroscopic Imaging of Oil Displacement in Dolomite," *J. Magn. Reson.*, **89**, 470 (1990).

Manickam, O., and G. M. Homsy, "Stability of Miscible Displacements in Porous Media with Nonmonotonic Viscosity Profiles," *Phys. Fluids A*, **5**, 1356 (1993).

Maudsley, A. A., S. K. Hilal, W. H. Perman, and H. E. Simon, "Spatially Resolved High Resolution Spectroscopy by 'Four-Dimensional' NMR," *J. Magn. Reson.*, **51**, 147 (1983).

Maudsley, A. A., Z. Wu, D. J. Meyerhoff, and M. W. Weiner, "Automated Processing for Proton Spectroscopic Imaging Using Water Reference Deconvolution," *Magn. Reson. Med.*, **31**, 589 (1994).

Meiburg, E., and G. M. Homsy, "Nonlinear Unstable Viscous Fingers in Hele-Shaw Flows. Part II: Numerical Simulation," *Phys. Fluids*, **31**, 429 (1988).

Moore, J. C., "The Overload Effect in Gel Permeation Chromatography," *Sep. Sci.*, **5**, 723 (1970).

Norton, T. T., and E. J. Fernandez, "Viscous Fingering in Size Exclusion Chromatography: Insights from Numerical Simulation," *Ind. Eng. Chem. Res.*, **35**, 2460 (1996).

Pearl, Z., M. Magaritz, and P. Bendel, "Nuclear Magnetic Resonance Imaging of Miscible Fingering in Porous Media," *Transp. Porous Media*, **12**, 107 (1993).

Perkins, T. K., and O. C. Johnston, "A Review of Diffusion and Dispersion in Porous Media," *Soc. Pet. Eng. J.*, **3**, 70 (1963).

Plante, L. D., P. R. Romano, and E. J. Fernandez, "Magnetic Resonance Imaging Analysis of Viscous Fingering in Chromatographic Separations," *Chem. Eng. Sci.*, **49**, 2229 (1994).

Posse, S., C. DeCarli, and D. Le Bihan, "Three-dimensional Echo-planar MR Spectroscopic Imaging at Short Echo Times in the Human Brain," *Radiology*, **192**, 733 (1994).

Purcell, E. M., H. C. Torrey, and R. V. Pound, "Resonance Absorption by Nuclear Magnetic Moments in a Solid," *Phys. Rev.*, **69**, 37 (1946).

Rothwell, W. P., and H. J. Vinegar, "Petrophysical Applications of NMR Imaging," *Appl. Opt.*, **24**, 3969 (1985).

Slobod, R. L., and R. A. Thomas, "Effect of Transverse Diffusion on Fingering in Miscible-Phase Displacement," *Soc. Pet. Eng. J.*, **3**, 9 (1963).

Stehling, M. K., R. Turner, and P. Mansfield, "Echo-Planar Imaging —Magnetic Resonance Imaging in a Fraction of a Second," *Science*, **254**, 43 (1991).

Stejskal, E. O., and J. E. Tanner, "Spin Diffusion Measurements: Spin Echoes in the Presence of a Time-Dependent Field Gradient," *J. Chem. Phys.*, **42**, 288 (1965).

Tan, C. T., and G. M. Homsy, "Stability of Miscible Displacements in Porous Media: Rectilinear Flow," *Phys. Fluids*, **29**, 3549 (1986).

Tan, C. T., and G. M. Homsy, "Simulation of Nonlinear Viscous Fingering in Miscible Displacement," *Phys. Fluids*, **31**, 1330 (1988).

Tchelepi, H. A. I. M., F. M. Orr, N. Rakotomalala, D. Salin, and R. Woumeni, "Dispersion, Permeability Heterogeneity, and Viscous Fingering: Acoustic Experimental Observations and Particle-tracking Simulations," *Phys. Fluids A*, **5**, 1558 (1993).

Vinegar, H. J., "X-Ray CT and NMR Imaging of Rocks," *J. Pet. Technol.*, **38**, 257 (1986).

Wankat, P. C., *Large Scale Adsorption and Chromatography*, CRC Press, Boca Raton, FL (1986).

Waugh, J. S., "Sensitivity in Fourier Transform NMR Spectroscopy of Slow Relaxing Systems," *J. Mol. Spectrosc.*, **35**, 298 (1970).

Yamamoto, S., M. Nomura, and Y. Sano, "Scaling Up of Medium-Performance Gel Filtration Chromatography of Proteins," *J. Chem. Eng. Japan*, **19**, 227 (1986).

Yortsos, Y. C., "Instabilities in Displacement Processes in Porous Media," *J. Phys. Condens. Matter*, **2**, SA 443 (1990).

Yortsos, Y. C., and M. Zeybek, "Dispersion Driven Instability in Miscible Displacement in Porous Media," *Phys. Fluids*, **31**, 3511 (1988).

Manuscript received Apr. 26, 1996, and revision received Aug. 2, 1996.